Bol. Soc. Paran. Mat.
©SPM – E-ISSN-2175-1188
SPM: www.spm.uem.br/bspm

(3s.) **v. 2025 (43) 3** : 1–21.
ISSN-0037-8712
doi:10.5269/bspm.78258

Reflection and Transmission of Elastic Waves at the Permeable Interface Between Fractured Porous Solid Saturated with Two Immiscible Pore Fluids and a Liquid Medium

Anil K. Vashishth and Sourab Kamboj*

ABSTRACT: The reflection and transmission of elastic waves at a permeable interface between a fluid half-space and a fractured porous solid (FPS) half-space saturated with two immiscible pore fluids, are examined within the framework of Volume Average Theory for porous solids. The FPS comprises a solid matrix saturated with two immiscible fluids within pores and a connected network of fractures in which five types of wave modes exist. Five transmitted waves in the FPS medium are attenuating waves. Energy partition across the interface is examined through the computation of reflection and transmission coefficients. Parametric analysis is conducted to evaluate the effects of partial pore opening at the interface, fractures, frequency, incidence angle, and pores permeabilities. The results of wave characteristics and energy distribution are highly sensitive to pore opening at the interface and multiphase fluid interactions within the fractured porous solid, thus offering key insights for subsurface imaging, reservoir evaluation, and acoustic monitoring.

Key Words: Volume Average Theory, fractured porous solid, double porosity, permeability, immiscible fluids, wave propagation, reflection and transmission.

Contents

1. Introduction

Wave propagation in porous media has emerged as a crucial area of study because of its diverse applications in environmental science, geophysics, engineering, and biomedical fields. Understanding of how incident acoustic waves interact with porous boundaries allows for better interpretation of seismic and acoustic signals in complex subsurface environments. The study of wave propagation behaviour at the interface of fluid-saturated porous solid is fundamental to applications in marine geophysics, underwater acoustics, reservoir exploration, and non-destructive testing. In oil engineering, studying reflection and transmission at the boundary of porous sedimentary rocks is critical for efficient hydrocarbon exploration and reservoir analysis. When seismic waves encounter porous rock layers, their reflection and refraction patterns provide valuable insights into subsurface structures, helping to identify potential oil and gas reservoirs. By analysing wave interactions in porous solids, engineers can estimate rock porosity, permeability, and fluid saturation, which are essential for evaluating reservoir quality.

* Corresponding author.

Submitted August 06, 2025. Published October 02, 2025

The theoretical foundation for modelling propagation of waves in porous media was laid by Biot [1,2,3,4], who introduced a comprehensive framework for describing the dynamics of fluid-saturated porous solids. Biot's theory predicts a slow (diffusive) compressional wave in addition to a fast compressional wave and a shear wave. Plona [5] confirmed the presence of the slow compressional wave through an experimental study. Building on Biot's Theory, Stoll and Kan [6] explored acoustic wave reflection from marine sediments, emphasising how permeability, porosity, and frame moduli influence the reflection coefficient. Their results, particularly in the context of low-frequency acoustic applications, revealed the significant role of viscous dissipation and the slow wave in energy loss mechanisms. Dutta and Ode [7] developed a theoretical model for the reflection and transmission of plane seismic waves at the boundary between two fluid-saturated porous solids. Their study focused on wave reflection and transmission at a single gas–brine contact within a shallow porous sandstone reservoir. Garg and Nayfeh [8] analysed wave propagation in fluid-saturated porous media by incorporating viscous and inertial effects to study both harmonic and transient responses. Later, Wu et al. [9] offered a detailed theoretical investigation into wave reflection and transmission at the fluid–porous boundary. By rigorously applying boundary conditions for both solid and fluid continuity, they provided analytical expressions for reflection-refraction coefficients. Denneman et al. [10] derived analytical expressions for wave reflection-refraction coefficients at a fluid–porous medium interface, showing that wave behaviour in water-saturated media closely resembles that in elastic solids, while air-saturated porous layers exhibit strong deviations due to acoustic impedance mismatch. Dai and Kuang [11] examined the reflection and refraction at the interface separating fluid half-space (FHS) and a double-porosity solid and examined the influence of dual pore structures on wave propagation behaviour. Their study provided insights into how the interaction between matrix and fracture systems in double porosity media affects wave reflection and transmission at fluid-solid boundaries. Vashishth and Sharma [12] explored the behaviour of acoustic waves at the boundary between a fluid half-space and a poroelastic ocean bottom, highlighting the influence of anisotropy, viscous dissipation, and pore structure on wave propagation and energy partitioning. Sharma [13] examined wave behaviour in materials exhibiting double porosity beneath a fluid half-space and found that wave-induced local fluid flow between the matrix and fractures leads to energy dissipation and frequency-dependent alterations in wave reflection. Geng et al. [14] demonstrate the effect of interfacial imperfections on wave reflection and transmission behaviour between FHS and porous solid.

Based on Volume Average Theory, Tuncay and Corapcioglu [15,16] developed constitutive relations for porous solids saturated with two immiscible fluids, capturing the coupled effects of fluid interactions and solid deformation. Later, Tuncay and Corapcioglu [17,18] proposed a model describing how the presence of fractures and two immiscible fluids influences the mechanical behaviour of porous materials, emphasising the role of fracture structure and fluid arrangement. Tomar and Arora [19] explored how elastic waves interact at the boundary between an elastic solid and a porous material containing two immiscible fluids, highlighting the impact of fluid saturation on wave reflection and transmission characteristics. Arora and Tomar [20] examined elastic wave interactions at the interface between a homogeneous solid and a fractured porous medium filled with immiscible fluids. Sharma and Kumar [21] investigated wave reflection at the free surface of a porous medium containing two immiscible fluids, showing the effect of the presence of dual fluids on the reflection characteristics of incident wave.

The above studies underline the importance and applications of studies on reflection and transmission of elastic waves at the boundary of porous solids saturated with one/two fluids, with or without fractures in the porous solids. The reflection-transmission phenomena at the boundary between a liquid half-space and a porous solid half-space, which incorporates the effects of fractures, double porosity and multiphase fluids with dual permeability based on Tuncay and Corapcioglu's Volume Average Theory, have not been studied so far.

Therefore, the present study focuses on the reflection and refraction of elastic waves at the permeable boundary separating a fluid half-space (FHS) and a fractured porous solid containing two immiscible pore fluids by taking into account the microstructure framework of Volume Average Theory (VAT). The micro structure of the porous medium includes a solid matrix framework permeated by two immiscible fluids and a connected fracture network. Five types of waves can propagate in such a medium which add the complexity to the mathematical model and the difficulty in obtaining its analytical solutions. Analytical expressions of energy ratios across the interface are obtained through the computation of reflection and

transmission coefficients. Numerical computation is done using MATLAB to examine the effects of partial pore opening of the interface, fractures, frequency, incidence angle, and permeabilities of the pores on the energy ratios. The schematic flow of the considered problem is illustrated in Figure 1.

2. Constitutive Equations

2.1. Fractured Porous Solid

Following Tuncay and Corapcioglu [17], the constitutive equations for fractured porous solids are given as follows:

$$\begin{aligned}
\langle\tau_s\rangle_{ij} &= \left[\left(a_{11}-\frac{2}{3}G_{fr}\right)s_{k,k}+a_{12}u_{k,k}+a_{13}v_{k,k}+a_{14}w_{k,k}\right]\delta_{ij}+G_{fr}(s_{i,j}+s_{j,i}),\\
\langle\tau_1\rangle_{ij} &= (a_{21}s_{k,k}+a_{22}u_{k,k}+a_{23}v_{k,k}+a_{24}w_{k,k})\delta_{ij},\\
\langle\tau_2\rangle_{ij} &= (a_{31}s_{k,k}+a_{32}u_{k,k}+a_{33}v_{k,k}+a_{34}w_{k,k})\delta_{ij},\\
\langle\tau_f\rangle_{ij} &= (a_{41}s_{k,k}+a_{42}u_{k,k}+a_{43}v_{k,k}+a_{44}w_{k,k})\delta_{ij},
\end{aligned} \tag{2.1}$$

where s_k, u_k, v_k, w_k $(k=1,2,3)$ denote the displacement components along the x_k-direction of the solid matrix, the non-wetting fluid in the primary pores, the wetting fluid in the primary pores, and the fluid in the fractures, respectively. Similarly, $\langle\tau_s\rangle_{ij}$, $\langle\tau_1\rangle_{ij}$, $\langle\tau_2\rangle_{ij}$, $\langle\tau_f\rangle_{ij}$ $(i,j=1,2,3)$ denote the stress components in the solid phase, the non-wetting fluid in the primary pores, the wetting fluid in the primary pores, and the fluid in the fractures, respectively. G_{fr} is shear modulus of the solid phase and δ_{ij} is Kronecker's delta. The expressions for elastic constants a_{mn} $(m,n=1,2,3,4)$ have been derived correctly here and are listed in Appendix A.

In the absence of body forces, the equations of motion are given by

$$\begin{aligned}
\langle\tau_s\rangle_{ij,j} &= \langle\rho_s\rangle\ddot{s}_i-e_1(\dot{u}_i-\dot{s}_i)-e_2(\dot{v}_i-\dot{s}_i)-e_3(\dot{w}_i-\dot{s}_i),\\
\langle\tau_1\rangle_{ij,j} &= \langle\rho_1\rangle\ddot{u}_i+e_1(\dot{u}_i-\dot{s}_i),\\
\langle\tau_2\rangle_{ij,j} &= \langle\rho_2\rangle\ddot{v}_i+e_2(\dot{v}_i-\dot{s}_i),\\
\langle\tau_f\rangle_{ij,j} &= \langle\rho_f\rangle\ddot{w}_i+e_3(\dot{w}_i-\dot{s}_i),
\end{aligned} \tag{2.2}$$

where $\langle\rho_s\rangle, \langle\rho_1\rangle, \langle\rho_2\rangle, \langle\rho_f\rangle$ are the average volume densities of the solid, non-wetting fluid, wetting phase fluid and fracture fluid, respectively.

The dissipation coefficients e_1, e_2 and e_3 are given by

$$e_1=\frac{\alpha_1^2\mu_1}{\chi_p\chi_{r1}}, \qquad e_2=\frac{\alpha_2^2\mu_2}{\chi_p\chi_{r2}}, \qquad e_3=\frac{\alpha_f^2\mu_f}{\chi_f}, \tag{2.3}$$

where α_1, α_2 and α_f are the volume fractions and μ_1, μ_2 and μ_f are the viscosities of non-wetting fluid, wetting fluid and fracture fluid, respectively. χ_p and χ_f are the permeability of primary pores and fractures respectively. χ_{r1} and χ_{r2} are the relative permeability of non-wetting and wetting phase fluid in primary pores.

Considering wave motion in the x_1–x_3 plane, the two-dimensional plane harmonic solutions to equation (2.2) can be formulated as follows:

$$\begin{aligned}
s_k &= a_k e^{(\iota\omega(t-\frac{x_1}{c}-qx_3))},\\
u_k &= b_k e^{(\iota\omega(t-\frac{x_1}{c}-qx_3))},\\
v_k &= c_k e^{(\iota\omega(t-\frac{x_1}{c}-qx_3))},\\
w_k &= d_k e^{(\iota\omega(t-\frac{x_1}{c}-qx_3))}, \quad (k=1,3),
\end{aligned} \tag{2.4}$$

where q denotes the unknown vertical slowness component, t is the time, ω represents the angular frequency, and c is the apparent phase velocity which can be written as

$$c=v^f/\sin\theta. \tag{2.5}$$

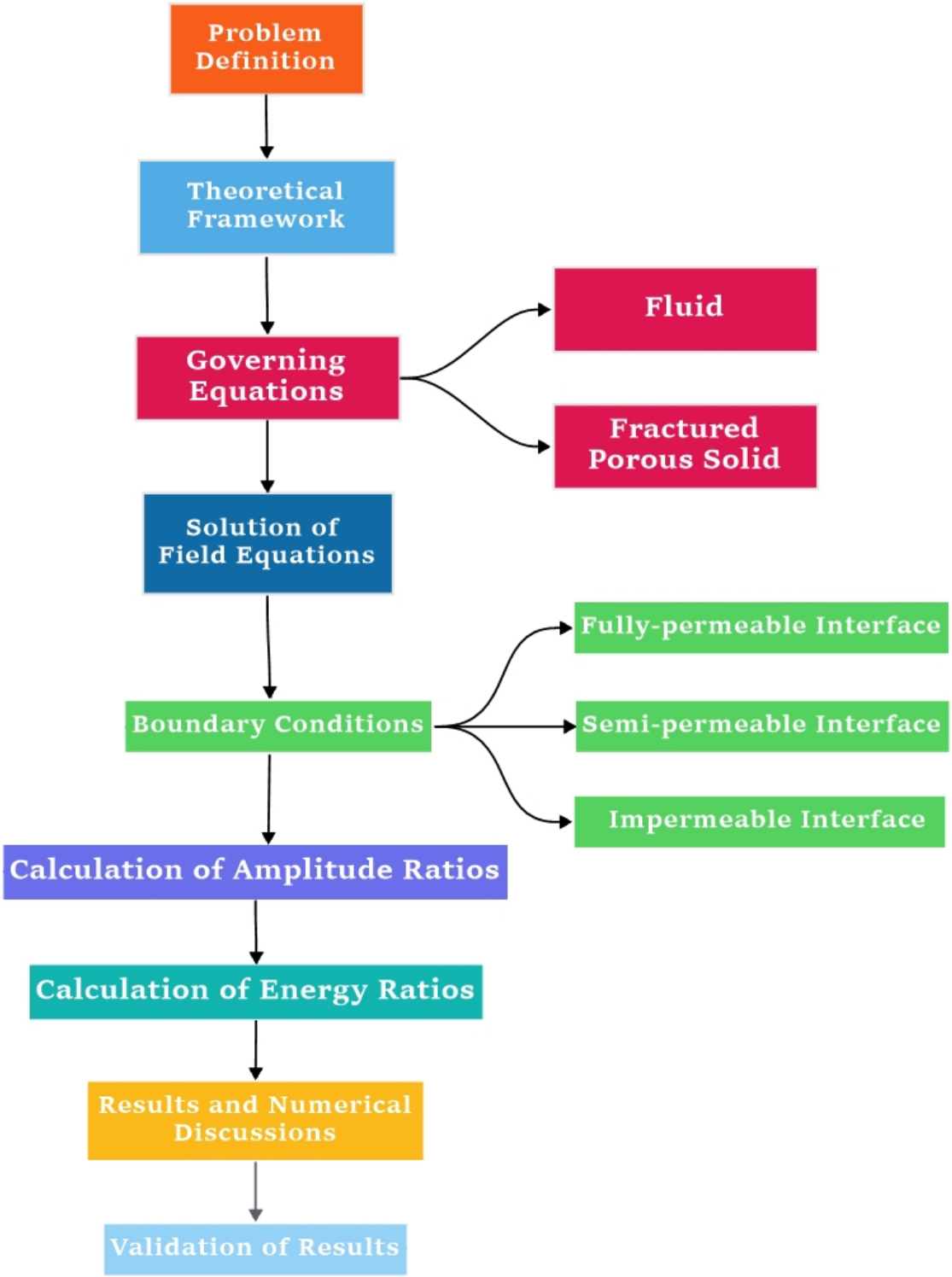

Figure 1: Flowchart of different phases/processes of the problem.

Here, v^f refers to the phase velocity of a wave in FHS that travels in the x_1–x_3 plane, moving in a direction that forms an angle θ with the x_3-axis. The quantities $a_1, a_3, b_1, b_3, c_1, c_3, d_1, d_3$ denote the amplitudes associated with the harmonic waves.

Using equation (2.4) in equation (2.2), we get a system of equations

$$\boldsymbol{\Gamma S} = 0, \tag{2.6}$$

where $\boldsymbol{S} = [a_1, a_3, b_1, b_3, c_1, c_3, d_1, d_3]^\top$, where '$\top$' denotes the transpose of the matrix, and the elements of the matrix $\Gamma_{8\times 8}$ are given in Appendix B.

The condition of non-trivial solution of (2.6) requires

$$|\boldsymbol{\Gamma}| = 0. \tag{2.7}$$

Equation(2.7) leads to

$$h_1 q^{10} + h_2 q^8 + h_3 q^6 + h_4 q^4 + h_5 q^2 + h_6 = 0, \tag{2.8}$$

where $h_1, h_2, ..., h_6$ are given in Appendix C.

The roots of equation (2.8) are complex. Out of 10 roots, five roots with negative real part represent the waves travelling along the negative x_3-axis (upgoing waves), and the roots with positive real part represent the waves travelling along the positive x_3-axis (downgoing waves). The roots are ordered in a such a way that $q(1)$, $q(2)$, $q(3)$, $q(4)$, $q(5)$ correspond to downgoing P_1, SV, P_2, P_3 and P_4 waves and $q(6)$, $q(7)$, $q(8)$, $q(9)$, $q(10)$ correspond to upgoing P_1, SV, P_2, P_3 and P_4 waves.

The wave amplitudes a_1, a_3, b_1, b_3, c_1, c_3, d_1, d_3 corresponding to the values of $q(j)$ are obtained from equation (2.6) as

$$\begin{aligned}
a_1(j) &= \frac{C(\Gamma_{81})_{q(j)}}{W_j}, \quad a_3(j) = \frac{C(\Gamma_{82})_{q(j)}}{W_j}, \quad b_1(j) = \frac{C(\Gamma_{83})_{q(j)}}{W_j}, \quad b_3(j) = \frac{C(\Gamma_{84})_{q(j)}}{W_j}, \\
c_1(j) &= \frac{C(\Gamma_{85})_{q(j)}}{W_j}, \quad c_3(j) = \frac{C(\Gamma_{86})_{q(j)}}{W_j}, \quad d_1(j) = \frac{C(\Gamma_{87})_{q(j)}}{W_j}, \quad d_3(j) = \frac{C(\Gamma_{88})_{q(j)}}{W_j},
\end{aligned} \tag{2.9}$$

with $(j = 1, 2, ..., 10)$, where $C(\Gamma_{mn})_{q(j)}$ denotes the cofactor of Γ_{mn} $(m, n = 1, 2, ..., 8)$ corresponding to $q(j)$ and

$W_j = \sqrt{\sum_{n=1}^{8} (C(\Gamma_{8n})_{q(j)})^2}$.

The displacement components can be written as

$$\begin{aligned}
s_1 &= \sum_{j=1}^{10} f(j) a_1(j) e^{(\iota\omega(t - \frac{x_1}{c} - q(j)x_3))}, \quad & s_3 &= \sum_{j=1}^{10} f(j) a_3(j) e^{(\iota\omega(t - \frac{x_1}{c} - q(j)x_3))}, \\
u_1 &= \sum_{j=1}^{10} f(j) b_1(j) e^{(\iota\omega(t - \frac{x_1}{c} - q(j)x_3))}, \quad & u_3 &= \sum_{j=1}^{10} f(j) b_3(j) e^{(\iota\omega(t - \frac{x_1}{c} - q(j)x_3))}, \\
v_1 &= \sum_{j=1}^{10} f(j) c_1(j) e^{(\iota\omega(t - \frac{x_1}{c} - q(j)x_3))}, \quad & v_3 &= \sum_{j=1}^{10} f(j) c_3(j) e^{(\iota\omega(t - \frac{x_1}{c} - q(j)x_3))}, \\
w_1 &= \sum_{j=1}^{10} f(j) d_1(j) e^{(\iota\omega(t - \frac{x_1}{c} - q(j)x_3))}, \quad & w_3 &= \sum_{j=1}^{10} f(j) d_3(j) e^{(\iota\omega(t - \frac{x_1}{c} - q(j)x_3))},
\end{aligned} \tag{2.10}$$

where $f(j)$ denotes the relative amplitudes of waves.

2.2. FHS

The displacement components and normal stress for a FHS are expressed as

$$\begin{aligned} U_1^f &= \sum_{l=1}^{2} n_1(l)A(l)e^{(\iota\omega(t-\frac{x_1}{c}-q^f(l)x_3))}, \\ U_3^f &= \sum_{l=1}^{2} n_3(l)A(l)e^{(\iota\omega(t-\frac{x_1}{c}-q^f(l)x_3))}, \\ \sigma_{33}^f &= \sum_{l=1}^{2} L_l A(l)e^{(\iota\omega(t-\frac{x_1}{c}-q^f(l)x_3))}, \end{aligned} \tag{2.11}$$

where

$$\begin{aligned} L_l &= \lambda^f(-\iota\omega)\left(\frac{n_1(l)}{c}+q^f(l)n_3(l)\right), \\ n_1(l) &= X_1(l)/X(l), n_3(l) = X_2(l)/X(l), \\ X_1(l) &= \lambda^f(q^f(l))^2-\rho^f, X_2(l) = \lambda^f\frac{q^f(l)}{c}, \\ X(l) = \sqrt{(X_1(l))^2+(X_2(l))^2}, \quad q^f(1) &= \frac{1}{c}\sqrt{\frac{c^2}{v^{f^2}}-1}, \quad q^f(2) = -\frac{1}{c}\sqrt{\frac{c^2}{v^{f^2}}-1}, \end{aligned} \tag{2.12}$$

where λ^f, ρ^f and v^f are the Lame's constant, the fluid density, and the longitudinal wave velocity within the fluid half-space, respectively.

3. Reflection and Transmission

Consider a fluid half-space lying over a fractured porous solid half-space that contains two immiscible viscous fluids. The boundary between the two regions lies along the plane $x_3 = 0$ in a rectangular coordinate system $(x_1, 0, x_3)$. An acoustic wave travels through the fluid and strikes the boundary at an angle θ from the vertical. The incident acoustic wave gives rise to a reflected wave in the fluid medium and five transmitted waves(P_1, SV, P_2, P_3, P_4) in the FPS medium. Here, the P_1, SV, and P_3 waves correspond to the fast compressional, shear, and slow compressional waves, respectively, as described in Biot's theory for a fluid-saturated porous medium. The P_2 wave is associated with the fracture fluid and disappears when the fracture volume fraction (α_f) is set to zero. The P_4 wave is associated with the second fluid in matrix pores.

The displacement components for the five downgoing transmitted waves can be written as

$$\begin{aligned} s_1 &= \sum_{j=1}^{5} f(j)a_1(j)e^{(\iota\omega(t-\frac{x_1}{c}-q(j)x_3))}, & s_3 &= \sum_{j=1}^{5} f(j)a_3(j)e^{(\iota\omega(t-\frac{x_1}{c}-q(j)x_3))}, \\ u_1 &= \sum_{j=1}^{5} f(j)b_1(j)e^{(\iota\omega(t-\frac{x_1}{c}-q(j)x_3))}, & u_3 &= \sum_{j=1}^{5} f(j)b_3(j)e^{(\iota\omega(t-\frac{x_1}{c}-q(j)x_3))}, \\ v_1 &= \sum_{j=1}^{5} f(j)c_1(j)e^{(\iota\omega(t-\frac{x_1}{c}-q(j)x_3))}, & v_3 &= \sum_{j=1}^{5} f(j)c_3(j)e^{(\iota\omega(t-\frac{x_1}{c}-q(j)x_3))}, \\ w_1 &= \sum_{j=1}^{5} f(j)d_1(j)e^{(\iota\omega(t-\frac{x_1}{c}-q(j)x_3))}, & w_3 &= \sum_{j=1}^{5} f(j)d_3(j)e^{(\iota\omega(t-\frac{x_1}{c}-q(j)x_3))}. \end{aligned} \tag{3.1}$$

4. Boundary Conditions

The appropriate boundary conditions at a permeable interface between the fluid and FPS are:

$$\begin{aligned}
&(i) && \langle t\rangle_{33} = \sigma^f_{33},\\
&(ii) && \langle \tau_s\rangle_{31} = 0,\\
&(iii) && \xi(\langle \tau_1\rangle_{33} - \alpha_1\langle t\rangle_{33}) = (1-\xi)\alpha_1 Z_1(\dot{u_3} - \dot{s_3}),\\
&(iv) && \xi(\langle \tau_2\rangle_{33} - \alpha_2\langle t\rangle_{33}) = (1-\xi)\alpha_2 Z_2(\dot{v_3} - \dot{s_3}),\\
&(v) && \xi(\langle \tau_f\rangle_{33} - \alpha_f\langle t\rangle_{33}) = (1-\xi)\alpha_f Z_f(\dot{w_3} - \dot{s_3}),\\
&(vi) && \alpha_s s_3 + \alpha_1 u_3 + \alpha_2 v_3 + \alpha_f w_3 = U^f_3,
\end{aligned} \tag{4.1}$$

where $\langle t\rangle_{33} = \langle \tau_s\rangle_{33} + \langle \tau_1\rangle_{33} + \langle \tau_2\rangle_{33} + \langle \tau_f\rangle_{33}$. Z_1, Z_2 and Z_f are surface flow impedance of the corresponding fluid phases. α_s is the volume fraction of solid phase in FPS. A parameter ξ takes into account, the permeability of the interface, i.e., the flow of fluid across the interface. The parameter $\xi = 0$ represents fully sealed surface pores, while $\xi = 1$ indicates a fully permeable interface. The intermediate value of ξ between 0 and 1 corresponds to a partially permeable interface.

Substituting stresses and displacements in the boundary conditions, we get a system of six inhomogeneous equations given by

$$\mathbf{H}\ \mathbf{Y} = \boldsymbol{G}, \tag{4.2}$$

where $\mathbf{H} = \begin{bmatrix} h_{11} & h_{12} & h_{13} & h_{14} & h_{15} & h_{16}\\ h_{21} & h_{22} & h_{23} & h_{24} & h_{25} & h_{26}\\ h_{31} & h_{32} & h_{33} & h_{34} & h_{35} & h_{36}\\ h_{41} & h_{42} & h_{43} & h_{44} & h_{45} & h_{46}\\ h_{51} & h_{52} & h_{53} & h_{54} & h_{55} & h_{56}\\ h_{61} & h_{62} & h_{63} & h_{64} & h_{65} & h_{66} \end{bmatrix}$, $\mathbf{Y} = \begin{bmatrix} \frac{f(1)}{A(1)}\\ \frac{f(2)}{A(1)}\\ \frac{f(3)}{A(1)}\\ \frac{f(4)}{A(1)}\\ \frac{f(5)}{A(1)}\\ \frac{A(2)}{A(1)} \end{bmatrix}$,

$$\boldsymbol{G} = \begin{bmatrix} g_1 \\ g_2 \\ g_3 \\ g_4 \\ g_5 \\ g_6 \end{bmatrix}, \text{ where}$$

$$\begin{aligned}
&g_1 = L_1, \quad g_2 = 0, \quad g_3 = 0, \quad g_4 = 0, \quad g_5 = 0, \quad g_6 = n_3(1),\\
&h_{11} = T_1, \quad h_{12} = T_2, \quad h_{13} = T_3, \quad h_{14} = T_4, \quad h_{15} = T_5, \quad h_{16} = -L_2,\\
&h_{21} = D_1, \quad h_{22} = D_2, \quad h_{23} = D_3, \quad h_{24} = D_4, \quad h_{25} = D_5, \quad h_{26} = 0,\\
&h_{31} = \xi\,(E_1 - \alpha_1 T_1) - (1-\xi)\alpha_1 Z_1(\iota\omega)\,(b_3(1) - a_3(1))\,,\\
&h_{32} = \xi\,(E_2 - \alpha_1 T_2) - (1-\xi)\alpha_1 Z_1(\iota\omega)\,(b_3(2) - a_3(2))\,,\\
&h_{33} = \xi\,(E_3 - \alpha_1 T_3) - (1-\xi)\alpha_1 Z_1(\iota\omega)\,(b_3(3) - a_3(3))\,,\\
&h_{34} = \xi\,(E_4 - \alpha_1 T_4) - (1-\xi)\alpha_1 Z_1(\iota\omega)\,(b_3(4) - a_3(4))\,,\\
&h_{35} = \xi\,(E_5 - \alpha_1 T_5) - (1-\xi)\alpha_1 Z_1(\iota\omega)\,(b_3(5) - a_3(5))\,,\\
&h_{36} = 0,\\
&h_{41} = \xi\,(F_1 - \alpha_2 T_1) - (1-\xi)\alpha_2 Z_2(\iota\omega)\,(c_3(1) - a_3(1))\,,\\
&h_{42} = \xi\,(F_2 - \alpha_2 T_2) - (1-\xi)\alpha_2 Z_2(\iota\omega)\,(c_3(2) - a_3(2))\,,\\
&h_{43} = \xi\,(F_3 - \alpha_2 T_3) - (1-\xi)\alpha_2 Z_2(\iota\omega)\,(c_3(3) - a_3(3))\,,\\
&h_{44} = \xi\,(F_4 - \alpha_2 T_4) - (1-\xi)\alpha_2 Z_2(\iota\omega)\,(c_3(4) - a_3(4))\,,\\
&h_{45} = \xi\,(F_5 - \alpha_2 T_5) - (1-\xi)\alpha_2 Z_2(\iota\omega)\,(c_3(5) - a_3(5))\,,\\
&h_{46} = 0,\\
&h_{51} = \xi\,(G_1 - \alpha_f T_1) - (1-\xi)\alpha_f Z_f(\iota\omega)\,(d_3(1) - a_3(1))\,,\\
&h_{52} = \xi\,(G_2 - \alpha_f T_2) - (1-\xi)\alpha_f Z_f(\iota\omega)\,(d_3(2) - a_3(2))\,,\\
&h_{53} = \xi\,(G_3 - \alpha_f T_3) - (1-\xi)\alpha_f Z_f(\iota\omega)\,(d_3(3) - a_3(3))\,,\\
&h_{54} = \xi\,(G_4 - \alpha_f T_4) - (1-\xi)\alpha_f Z_f(\iota\omega)\,(d_3(4) - a_3(4))\,,\\
&h_{55} = \xi\,(G_5 - \alpha_f T_5) - (1-\xi)\alpha_f Z_f(\iota\omega)\,(d_3(5) - a_3(5))\,,\\
&h_{56} = 0,\\
&h_{61} = \alpha_s\, a_3(1) + \alpha_1\, b_3(1) + \alpha_2\, c_3(1) + \alpha_f\, d_3(1),\\
&h_{62} = \alpha_s\, a_3(2) + \alpha_1\, b_3(2) + \alpha_2\, c_3(2) + \alpha_f\, d_3(2),\\
&h_{63} = \alpha_s\, a_3(3) + \alpha_1\, b_3(3) + \alpha_2\, c_3(3) + \alpha_f\, d_3(3),\\
&h_{64} = \alpha_s\, a_3(4) + \alpha_1\, b_3(4) + \alpha_2\, c_3(4) + \alpha_f\, d_3(4),\\
&h_{65} = \alpha_s\, a_3(5) + \alpha_1\, b_3(5) + \alpha_2\, c_3(5) + \alpha_f\, d_3(5),\\
&h_{66} = -n_3(2),\\
&T_1 = C_1 + F_1 + E_1 + G_1, \quad T_2 = C_2 + F_2 + E_2 + G_2,\\
&T_3 = C_3 + F_3 + E_3 + G_3, \quad T_4 = C_4 + F_4 + E_4 + G_4,\\
&T_5 = C_5 + F_5 + E_5 + G_5,
\end{aligned}$$

$$C_j = (-\iota\omega)\left[a_{11}\frac{a_1(j)}{c} + (a_{11}+2G_{fr})a_3(j)q(j) + a_{12}\left(\frac{b_1(j)}{c} + b_3(j)q(j)\right)\right.$$
$$\left. + a_{13}\left(\frac{c_1(j)}{c} + c_3(j)q(j)\right) + a_{14}\left(\frac{d_1(j)}{c} + d_3(j)q(j)\right)\right],$$
$$D_j = (-\iota\omega)G_{fr}\left[a_1(j)q(j) + \frac{a_3(j)}{c}\right],$$
$$E_j = (-\iota\omega)\left[a_{21}\left(\frac{a_1(j)}{c} + a_3(j)q(j)\right) + a_{22}\left(\frac{b_1(j)}{c} + b_3(j)q(j)\right)\right.$$
$$\left. + a_{23}\left(\frac{c_1(j)}{c} + c_3(j)q(j)\right) + a_{24}\left(\frac{d_1(j)}{c} + d_3(j)q(j)\right)\right],$$
$$F_j = (-\iota\omega)\left[a_{31}\left(\frac{a_1(j)}{c} + a_3(j)q(j)\right) + a_{32}\left(\frac{b_1(j)}{c} + b_3(j)q(j)\right)\right.$$
$$\left. + a_{33}\left(\frac{c_1(j)}{c} + c_3(j)q(j)\right) + a_{34}\left(\frac{d_1(j)}{c} + d_3(j)q(j)\right)\right],$$

$$G_j = (-\iota\omega)\left[a_{41}\left(\frac{a_1(j)}{c} + a_3(j)q(j)\right) + a_{42}\left(\frac{b_1(j)}{c} + b_3(j)q(j)\right)\right.$$
$$\left. + a_{43}\left(\frac{c_1(j)}{c} + c_3(j)q(j)\right) + a_{44}\left(\frac{d_1(j)}{c} + d_3(j)q(j)\right)\right]. \tag{4.3}$$

5. Energy Ratios

The average energy flux for transmitted waves in the FPS medium for a surface with a normal along the x_3-direction is given by [22],

$$\langle Q^*_{jk}\rangle = \Re(\langle\tau_s\rangle^{(j)}_{31})\Re(\dot{s}^{(k)}_1) + \Re(\langle\tau_s\rangle^{(j)}_{33})\Re(\dot{s}^{(k)}_3) + \Re(\langle\tau_1\rangle^{(j)}_{33})\Re(\dot{u}^{(k)}_3) + \Re(\langle\tau_2\rangle^{(j)}_{33})\Re(\dot{v}^{(k)}_3)$$
$$+ \Re(\langle\tau_f\rangle^{(j)}_{33})\Re(\dot{w}^{(k)}_3), (j,k=1,2,3,4,5). \tag{5.1}$$

On solving equation (5.1), we obtained

$$\langle Q^*_{jk}\rangle = \Re\left[(-\iota\omega)\left(D_j\overline{a_1(k)} + C_j\overline{a_3(k)} + E_j\overline{b_3(k)} + F_j\overline{c_3(k)} + G_j\overline{d_3(k)}\right)Y_j\overline{Y}_k\right], (j,k=1,2,3,4,5), \tag{5.2}$$

where $Y_1 = \dfrac{f(1)}{A(1)}$, $Y_2 = \dfrac{f(2)}{A(1)}$, $Y_3 = \dfrac{f(3)}{A(1)}$, $Y_4 = \dfrac{f(4)}{A(1)}$, and $Y_5 = \dfrac{f(5)}{A(1)}$. The complex conjugate of an entity is denoted by placing a bar over it.

The mean energy flux of incident and reflected waves in FHS is

$$\langle F_I\rangle = -(\iota\omega)\ n_3(1)L_1|A(1)|^2, \tag{5.3}$$

and

$$\langle F_R\rangle = -(\iota\omega)\ n_3(2)L_2|A(2)|^2. \tag{5.4}$$

The energy ratio of the reflected wave is given by

$$E_R = \left|\frac{A(2)}{A(1)}\right|^2. \tag{5.5}$$

The energy ratios of the transmitted waves are determined as follows

$$E_{jk} = \frac{\langle Q^*_{jk}\rangle}{\langle F_I\rangle}, (j,k=1,2,3,4,5). \tag{5.6}$$

On solving equation (5.6), the energy ratios E_{11}, E_{22}, E_{33}, E_{44}, and E_{55}, corresponding to the transmitted waves P_1, SV, P_2, P_3, and P_4, respectively, are given by

$$
\begin{aligned}
E_{11} &= \Re\left[\frac{(-\iota\omega)\left(D_1\,\overline{a_1(1)} + C_1\,\overline{a_3(1)} + E_1\,\overline{b_3(1)} + F_1\,\overline{c_3(1)} + G_1\,\overline{d_3(1)}\right)|Y_1|^2}{(-\iota\omega)\,n_3(1)\,L_1\,|A(1)|^2}\right],\\
E_{22} &= \Re\left[\frac{(-\iota\omega)\left(D_2\,\overline{a_1(2)} + C_2\,\overline{a_3(2)} + E_2\,\overline{b_3(2)} + F_2\,\overline{c_3(2)} + G_2\,\overline{d_3(2)}\right)|Y_2|^2}{(-\iota\omega)\,n_3(1)\,L_1\,|A(1)|^2}\right],\\
E_{33} &= \Re\left[\frac{(-\iota\omega)\left(D_3\,\overline{a_1(3)} + C_3\,\overline{a_3(3)} + E_3\,\overline{b_3(3)} + F_3\,\overline{c_3(3)} + G_3\,\overline{d_3(3)}\right)|Y_3|^2}{(-\iota\omega)\,n_3(1)\,L_1\,|A(1)|^2}\right],\\
E_{44} &= \Re\left[\frac{(-\iota\omega)\left(D_4\,\overline{a_1(4)} + C_4\,\overline{a_3(4)} + E_4\,\overline{b_3(4)} + F_4\,\overline{c_3(4)} + G_4\,\overline{d_3(4)}\right)|Y_4|^2}{(-\iota\omega)\,n_3(1)\,L_1\,|A(1)|^2}\right],\\
E_{55} &= \Re\left[\frac{(-\iota\omega)\left(D_5\,\overline{a_1(5)} + C_5\,\overline{a_3(5)} + E_5\,\overline{b_3(5)} + F_5\,\overline{c_3(5)} + G_5\,\overline{d_3(5)}\right)|Y_5|^2}{(-\iota\omega)\,n_3(1)\,L_1\,|A(1)|^2}\right].
\end{aligned}
\tag{5.7}
$$

The total interaction energy arising from the mutual interactions among the transmitted waves is expressed as

$$
E_{int} = \sum_{j=1}^{5}\left(\sum_{k=1}^{5} E_{jk} - E_{jj}\right). \tag{5.8}
$$

6. Numerical Discussions

For numerical computation, the elastic parameters for a North Sea sandstone saturated with CO_2 and water are considered and are given in Table 1. The values for surface flow impedance are $Z_1 = 10^2\,\mathrm{Pa\cdot s\cdot m^{-1}}$, $Z_2 = 10^4\,\mathrm{Pa\cdot s\cdot m^{-1}}$, and $Z_f = 10\,\mathrm{Pa\cdot s\cdot m^{-1}}$. Furthermore, $\rho^f = 990$ kg/m^3 and $\lambda^f = 2.3\times10^9$ GPa are chosen for FHS.

Table 1: FPS medium parameters [8].

Parameter	Description	Value
$\langle\rho_s\rangle$	Average density of solid grains	$\alpha_s \times 2650$ kg/m^3
$\langle\rho_1\rangle$	Average density of CO_2 in matrix pores	$\alpha_1 \times 103$ kg/m^3
$\langle\rho_2\rangle$	Average density of water in matrix pores	$\alpha_2 \times 990$ kg/m^3
$\langle\rho_f\rangle$	Average density of water in fractures	$\alpha_f \times 990$ kg/m^3
χ_p	Matrix permeability	10^{-16} m^2
χ_f	Fracture permeability	10^{-12} m^2
K_s	Bulk modulus of solid grains	36 GPa
K_{fr}	Bulk modulus of fractured medium	6.25 GPa
K_{frm}	Bulk modulus of non-fractured blocks	12 GPa
G_{fr}	Shear modulus of fractured medium	9 GPa
μ_1	Viscosity of CO_2	1.8×10^{-5} Pa$\cdot$s
μ_2	Viscosity of water in matrix pores	10^{-3} Pa$\cdot$s
μ_f	Viscosity of water in fractures	10^{-3} Pa$\cdot$s
K_1	Bulk modulus of CO_2	3.7 MPa
K_2	Bulk modulus of water in matrix pores	2.3 GPa
K_f	Bulk modulus of water in fractures	2.3 GPa
P_{cap}	Capillary pressure	$0.1S_1$MPa

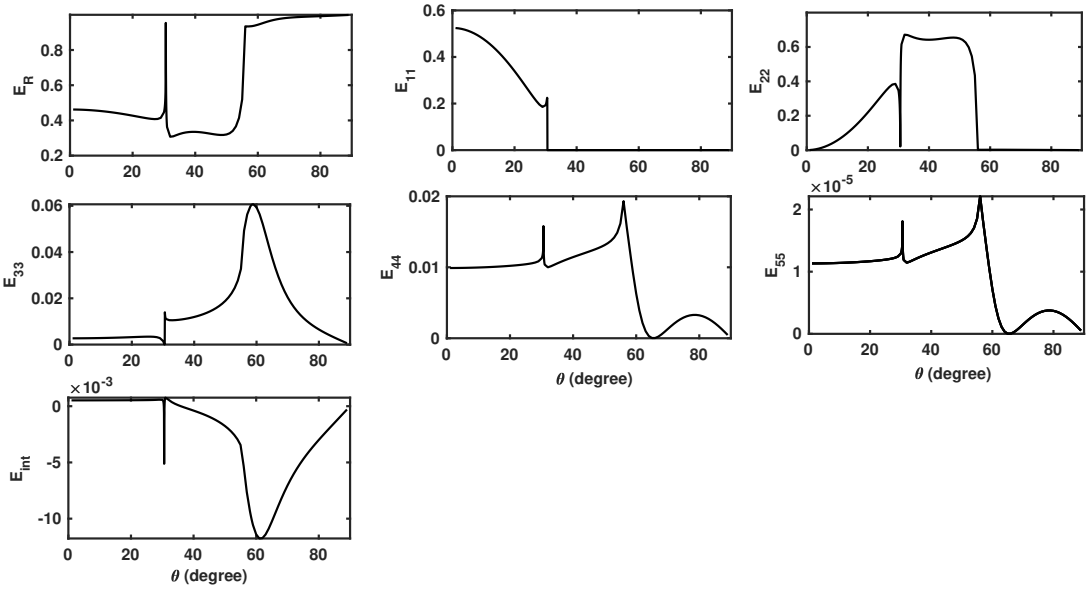

Figure 2: Variation in energy ratios of reflected(P), transmitted(P_1, SV, P_2, P_3, P_4) and interaction energy with θ ; $\alpha_s = 0.89$; $\alpha_1 = 0.05$; $\alpha_2 = 0.05$; $\alpha_f = 0.01$; $\xi = 0.5$; $\omega = 2\pi \times 20Hz$.

Figure 2 shows the distribution of incident wave energy among reflected and transmitted waves with the angle of incidence. The pores at the interface are assumed to be partially open ($\xi = 0.5$). From the figure, it is evident that the first critical angle, corresponding to the transmitted P_1 wave (θ_{cP}), is 30.6°, while the second critical angle, associated with the transmitted SV wave (θ_{cSV}), is 56°. Before the critical angles, the energy ratios associated with the reflected P wave and transmitted P_1 wave show a decreasing trend, whereas the transmitted SV wave's energy ratio rises. At the critical angle, $\theta_{cP} = 30.6°$, the energy shares of the transmitted P_1, P_2, and SV waves reach their minimum values, while the reflected P wave energy ratio reaches its maximum. The energy ratios corresponding to P_2 and P_3 waves show pronounced peaks in the vicinity of the critical angle θ_{cP}. This phenomenon is attributed to an enhanced mode conversion near the critical angle. Beyond this critical angle θ_{cP}, the transmitted P_1 wave becomes evanescent. As the incident angle continues to increase, the energy associated with the transmitted SV wave rises until it reaches the critical angle for SV wave transmission ($\theta_{cSV} = 56°$). Beyond this angle, the SV wave also becomes evanescent. A noticeable peak in the energy ratios of the slow waves (P_2, P_3, and P_4) is observed near the critical angle of the SV wave. Consequently, for incident angles greater than 56°, no significant energy is transmitted into either the fast P_1 wave or SV wave modes within the FPS medium.

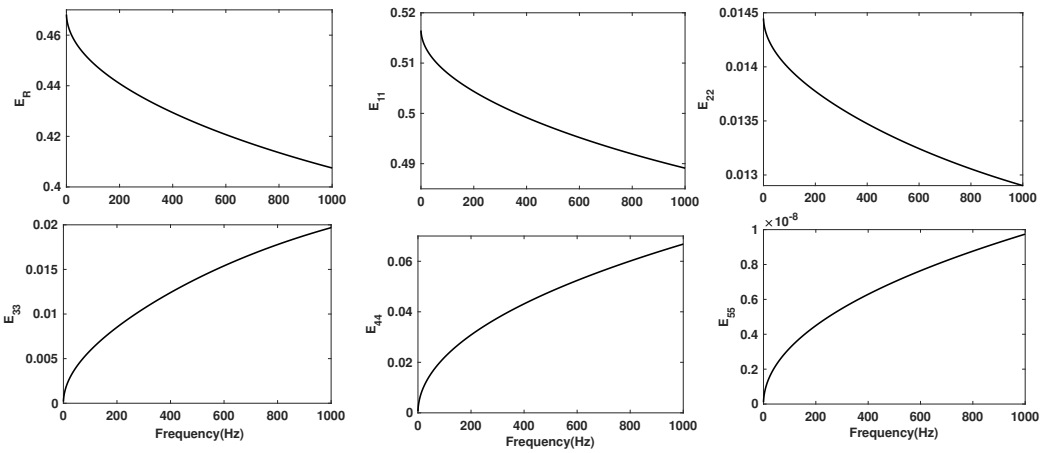

Figure 3: Effect of frequency on energy ratios of reflected(P), transmitted(P_1, SV, P_2, P_3, P_4); $\theta = 5°$; $\alpha_s = 0.89$; $\alpha_1 = 0.05$; $\alpha_2 = 0.05$; $\alpha_f = 0.01$; $\xi = 0.5$.

Figure 3 shows the effect of frequency on the energy distribution. With the increase in frequency, the distribution of energy among wave modes in a fractured porous solid undergoes a notable shift. The energy of the reflected P wave, transmitted P_1, and SV wave tends to decrease, indicating reduced efficiency in energy transmission through fast wave modes at higher frequencies. This behaviour is attributed to enhanced viscous interactions between the pore fluids and solid matrix, which become more pronounced as frequency rises. These interactions increase attenuation in fast modes while promoting the excitation of slow compressional waves. Consequently, the energy share associated with matrix-related slow waves (P_3, P_4) and fracture-dominated modes (P_2) increases significantly with frequency.

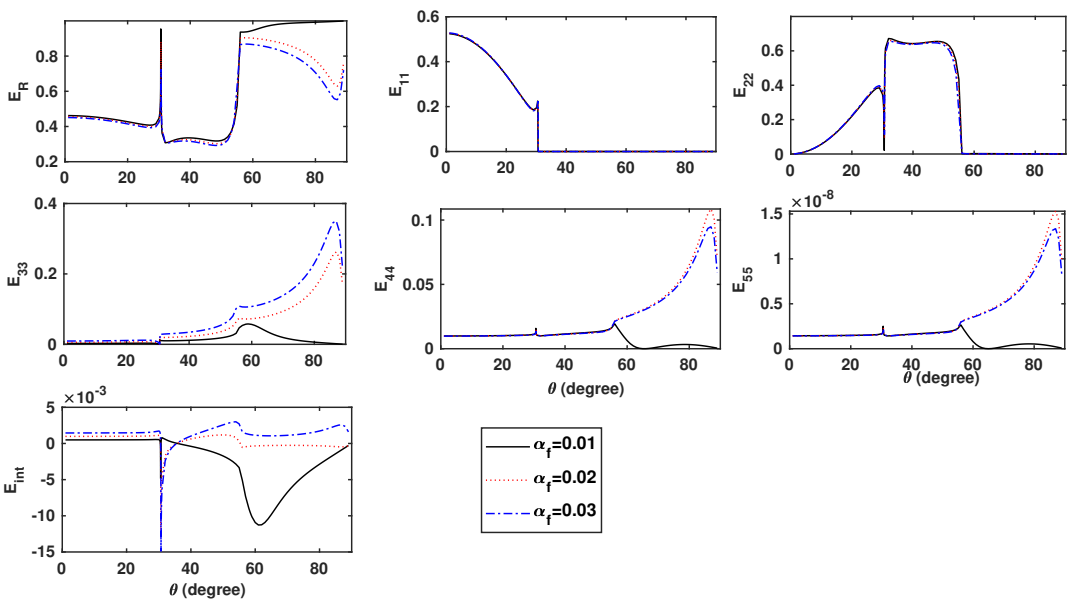

Figure 4: Effect of fracture volume fraction(α_f) on energy ratios of reflected(P), transmitted(P_1, SV, P_2, P_3, P_4) waves and interaction energy with θ; $\alpha_s = 0.90 - \alpha_f$; $\alpha_1 = 0.05$; $\alpha_2 = 0.05$; $\xi = 0.5$; $\omega = 2\pi \times 20Hz$.

Figure 4 depicts the impact of fractures on the energy distribution between the reflected and transmitted waves. As the fractures increase in the FPS medium, the energy of reflected P wave and SV declines, while a significant increase in the energy of P_2 wave is observed. Notably, this increase in the energy of P_2 becomes more pronounced for incident angles greater than 56°. Energy share of slow P_3 and P_4 waves associated with matrix pores also declines with increase in fractures up to $\theta < 56°$, after this angle, their share increases significantly. It is noted that the amount by which the energy ratio of the reflected wave decreases is the same amount of energy increment in the P_2 and P_3 waves. The observed increase in energy share of the slow waves beyond $\theta > 56°$ can be attributed to enhanced interaction and coupling between the slow wave modes(P_2, P_3 and P_4), particularly when fast wave modes become evanescent.

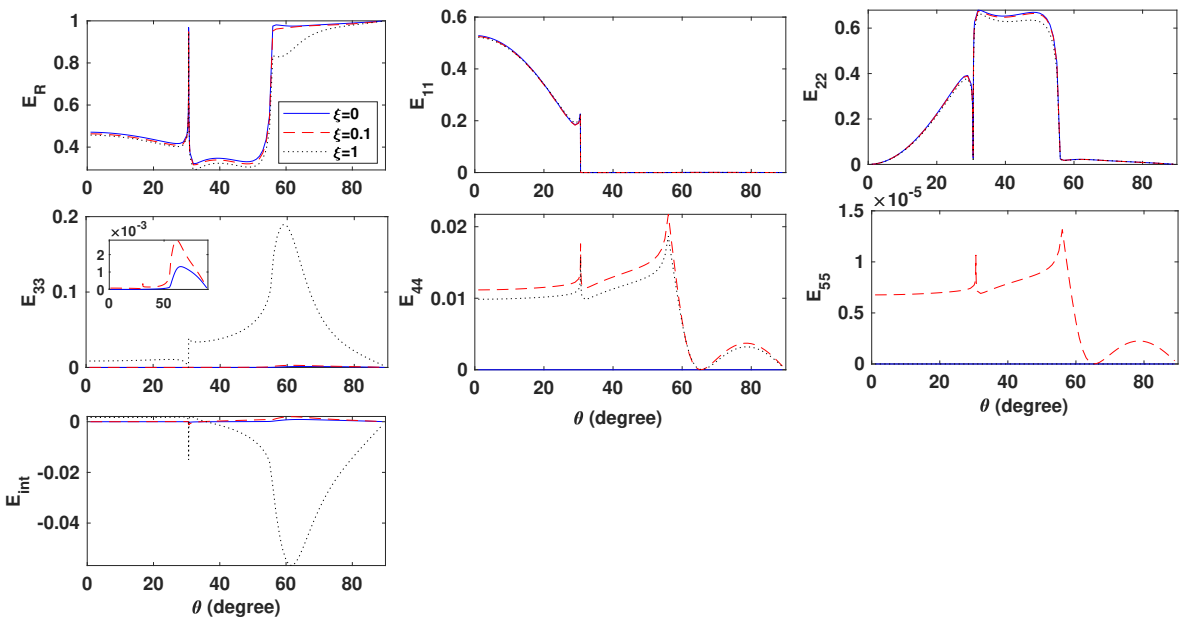

Figure 5: Effect of varying the pore-opening parameter ξ on energy ratios of reflected(P), transmitted(P_1, SV, P_2, P_3, P_4) waves and interaction energy with θ; $\alpha_s = 0.89$; $\alpha_1 = 0.05$; $\alpha_2 = 0.05$; $\alpha_f = 0.01$; $\xi = 0.5$; $\omega = 2\pi \times 20Hz$.

Figure 5 demonstrates the influence of pore opening at the interface on the energy distribution of transmitted waves. The parameter $\xi = 0$ represents a fully sealed interface, while $\xi = 1$ corresponds to fully open pores at the interface. As ξ increases beyond 0, enhanced fluid exchange across the interface enables greater transmission of wave energy into the FPS medium. This results in a notable rise in the energy of the second compressional wave (P_2), which becomes dominant among the slow wave modes when the pores are fully open at the interface. A negligible effect is observed on the energy ratio of the transmitted fast P_1, while the transmitted SV wave shows a slight decrease in energy. Interestingly, for partial pore opening (e.g., $\xi = 0.1$), the energy of P_3 and P_4 waves is higher than that observed in both the sealed and fully open cases. This non-monotonic behaviour is attributed to the complex interplay between pore opening at the interface and wave-induced fluid motion. The enhanced permeability of the fracture network, relative to the matrix, plays a crucial role in facilitating the observed energy redistribution.

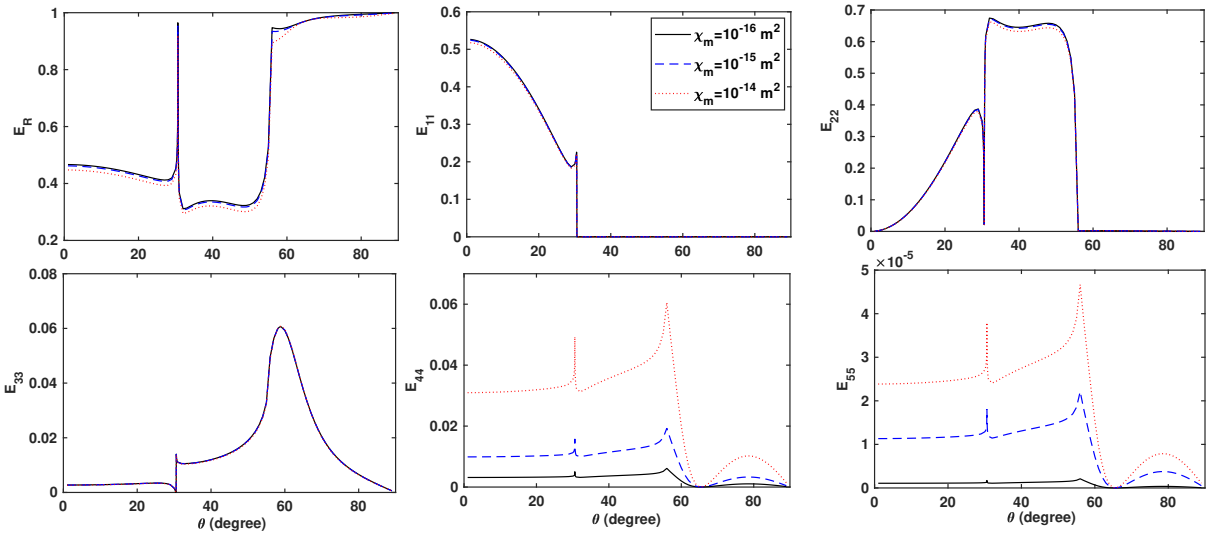

Figure 6: Effect of different matrix permeability(χ_m) on energy ratios of reflected(P), transmitted(P_1, SV, P_2, P_3, P_4) waves with θ; $\alpha_s = 0.89$; $\alpha_1 = 0.05$; $\alpha_2 = 0.05$; $\alpha_f = 0.01$; $\xi = 0.5$; $\omega = 2\pi \times 20Hz$.

Figure 6 shows the impact of matrix pore permeability on the energy distribution between various wave modes. As matrix permeability increases, the energy ratios associated with the slow compressional waves P_3 and P_4 show a noticeable rise. In contrast, the energy shares of the reflected P wave, transmitted fast compressional wave (P_1), and shear wave (SV) gradually decrease. The energy ratio corresponding to the fracture-related wave (P_2) remains unaffected by variations in matrix permeability.

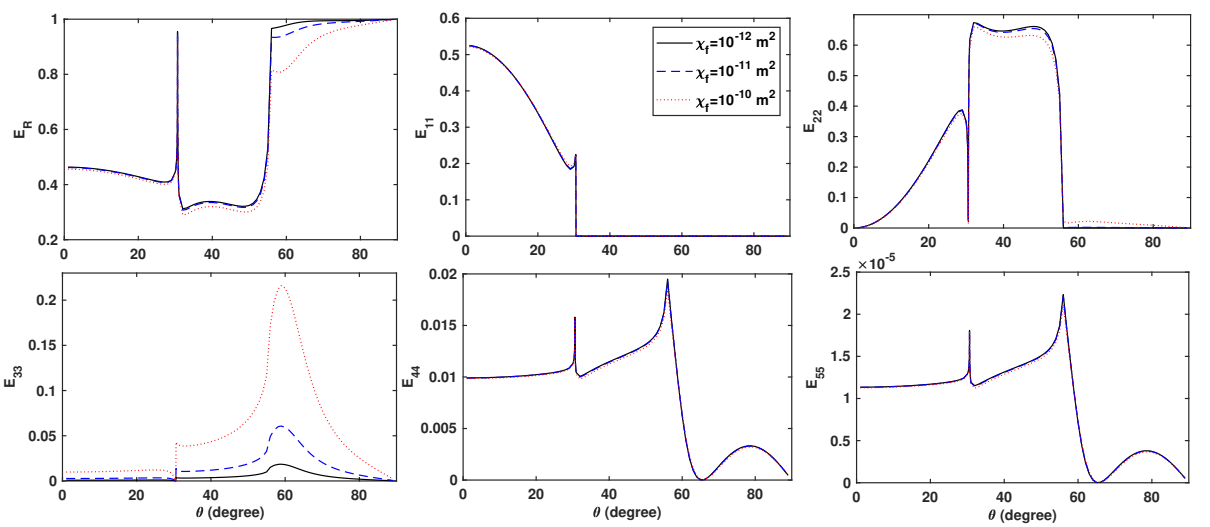

Figure 7: Effect of different fracture permeability(χ_f) on energy ratios of reflected(P), transmitted(P_1, SV, P_2, P_3, P_4) waves with θ; $\alpha_s = 0.89$; $\alpha_1 = 0.05$; $\alpha_2 = 0.05$; $\alpha_f = 0.01$; $\xi = 0.5$; $\omega = 2\pi \times 20Hz$.

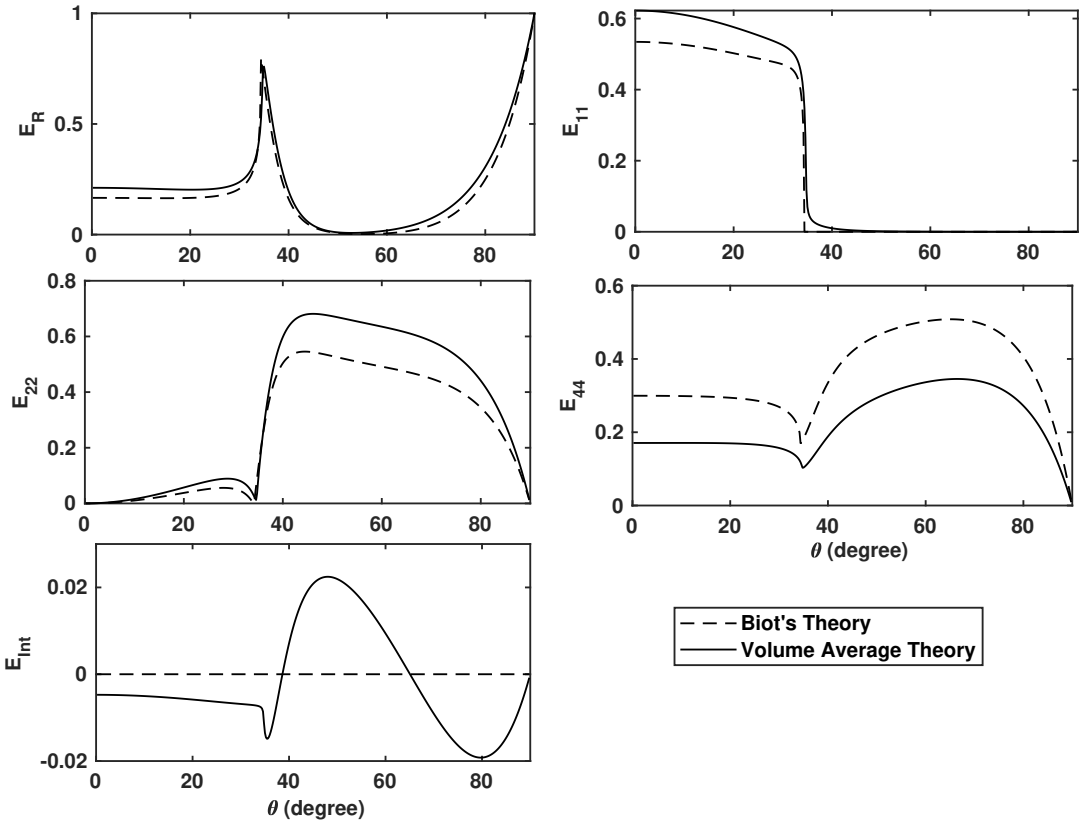

Figure 8: Comparison of energy ratios calculated by Biot's Theory and the Volume Average Theory as a function of the incidence angle θ; $\omega = 2\pi \times 100Hz$; $\alpha_s = 0.62$; $\alpha_2 = 0.38$.

Figure 7 demonstrates the effect of fracture permeability on the energy distribution. As the fracture permeability increases, the energy share of P_2 increases noticeably, indicating stronger fluid mobility through the fracture pores. In contrast to the P_2 wave, the energies of the reflected and all other transmitted waves decrease. This redistribution of energy highlights the dominant role of fractures in the FPS medium. Therefore, the presence of fractures markedly alters the propagation characteristics of waves in porous solids.

6.1. Reduced Case

The fractured porous solid (FPS) model may be reduced to a classical porous solid saturated with a single fluid by setting $\alpha_1 = 0$ and $\alpha_f = 0$. Under these conditions, the influence of the fracture network and one fluid phase is eliminated, effectively reducing the system to a two-phase porous medium. In this simplified scenario, three refracted wave modes P_1, SV, and P_3 are present within the porous solid. According to Biot's theory, the P_3 wave corresponds to the slow compressional wave. The P_2 wave, associated with fracture networks, and the P_4 wave, associated with the gaseous phase in the primary pores of the FPS medium, no longer exist in this case. A comparison of energy ratios predicted by Biot's Theory and the Volume Average Theory is presented in Figure 8. The findings are qualitatively consistent with those reported by Wu et al. [9] using Biot's theory. When the volume average approach is employed, a higher energy share is predicted for the transmitted P_1 and SV waves. In contrast, Biot's theory indicates a greater energy contribution from the refracted P_2 wave. Furthermore, Wu et al. [9] neglected energy dissipation within the medium, whereas this paper incorporates it. Consequently, some energy is lost as a result of wave interactions.

7. Conclusions

The reflection-transmission phenomena at the interface between a FHS and a FPSHS, which incorporates the effects of fractures, double porosity, and multiphase fluids with dual permeability based on Volume Average Theory, is studied. The following conclusions are drawn based on the above study.

- At critical angle, $\theta_{cP} = 30.6°$, the energy ratios of transmitted P_1, P_2 and SV waves reach their minimum values, while the reflected P wave energy ratio reaches its maximum. Beyond the critical angle θ_{cP}, the transmitted P_1 wave becomes evanescent.
- As the incident angle continues to increase, the energy associated with the transmitted SV wave rises until it reaches the critical angle for SV wave transmission ($\theta_{cSV} = 56°$). Beyond this angle, the SV wave also becomes evanescent. A noticeable peak in the energy ratios of the slow compressional waves (P_2, P_3, and P_4) is observed near the critical angle of the SV wave.
- As frequency increases, the energy ratios of the reflected P wave, transmitted P_1, and SV wave gradually decline, indicating diminished energy transmission through fast wave modes. This behaviour results from stronger viscous interactions between the pore fluids and the solid matrix at elevated frequencies.
- The energy ratios of slow waves (P_2, P_3, P_4) increases significantly with frequency.
- As the fractures volume fraction increases in the FPS medium, the energy ratio of the reflected P wave and SV decreases while a significant increase in the energy ratio of the P_2 wave is observed. Notably, this increase in the energy ratio of the P_2 wave becomes more significant for incident angles greater than 56°.
- For partial opening of the pores at the interface of the fluid-FPS interface, the energy ratios of the slow compressional waves (P_3 and P_4) are higher than those observed in both the sealed and fully open cases.
- As matrix permeability increases, the energy ratios associated P_3 and P_4 waves show a noticeable increase. In contrast, the energy shares of the reflected P wave, transmitted fast compressional wave (P_1), and shear wave (SV) gradually decrease.
- As the permeability of the fractures increases, the energy share of the P_2 increases noticeably, indicating stronger fluid mobility through the fracture pores.
- The observed frequency-dependent decline in fast wave energy transmission, driven by fluid-solid viscous interactions, provides key insights for improving subsurface imaging, reservoir characterisation, and acoustic monitoring in fractured porous media.

Acknowledgement

We thank the organizers of the "International Conference on Mathematical Sciences and Computing Innovations and Applications (ICMSC-2025) jointly organized by Department of Mathematics North Eastern Regional Institute of Science and Technology (NERIST) and Department of Mathematics National Institute of Technology (NIT), Uttarakhand held during June 26-28, 2025".

The authors sincerely thank UGC, India, for awarding Mr. Sourab Kamboj a JRF, UGC-JRF Award Ref. No. 191620014843.

Appendix A

$a_{11} = -\alpha_s(J_{32} + J_{33})$,$a_{12} = -\alpha_s J_{34}, a_{13} = -\alpha_s J_{35}, a_{14} = -\alpha_s J_{37}$,
$a_{21} = -S_1\alpha_p(J_{42} + J_{43}), a_{22} = -S_1\alpha_p J_{44}, a_{23} = -S_1\alpha_p J_{45}, a_{24} = S_1\alpha_p J_{47}$,
$a_{31} = -(1 - S_1)\alpha_p(J_{52} + J_{53}), a_{32} = -(1 - S_1)\alpha_p J_{54}, a_{33} = -(1 - S_1)\alpha_p J_{55}, a_{34} = -(1 - S_1)\alpha_p J_{57}$,
$a_{41} = -\alpha_f(J_{72} + J_{73}), a_{42} = -\alpha_f J_{74}, a_{43} = -\alpha_f J_{75}, a_{44} = -\alpha_f J_{77}$,

$J_{11} = R_{11} - J_{61}\alpha_p(R_{14} + R_{15}) - J_{71}R_{12}E_2,$
$J_{12} = R_{12} - J_{62}\alpha_p(R_{14} + R_{15}) - J_{72}R_{12}E_2,$
$J_{13} = R_{13} - J_{63}\alpha_p(R_{14} + R_{15}) - J_{73}R_{12}E_2,$
$J_{14} = R_{14} - J_{64}\alpha_p(R_{14} + R_{15}) - J_{74}R_{12}E_2,$
$J_{15} = R_{15} - J_{65}\alpha_p(R_{14} + R_{15}) - J_{75}R_{12}E_2,$
$J_{21} = R_{21} - J_{61}\alpha_p(R_{24} + R_{25}) - J_{71}R_{22}E_2,$
$J_{22} = R_{22} - J_{62}\alpha_p(R_{24} + R_{25}) - J_{72}R_{22}E_2,$
$J_{23} = R_{23} - J_{63}\alpha_p(R_{24} + R_{25}) - J_{73}R_{22}E_2,$
$J_{24} = R_{24} - J_{64}\alpha_p(R_{24} + R_{25}) - J_{74}R_{22}E_2,$
$J_{25} = R_{25} - J_{65}\alpha_p(R_{24} + R_{25}) - J_{75}R_{22}E_2,$
$J_{31} = R_{31} - J_{61}\alpha_p(R_{34} + R_{35}) - J_{71}R_{32}E_2,$
$J_{32} = R_{32} - J_{62}\alpha_p(R_{34} + R_{35}) - J_{72}R_{32}E_2,$
$J_{33} = R_{33} - J_{63}\alpha_p(R_{34} + R_{35}) - J_{73}R_{32}E_2,$
$J_{34} = R_{34} - J_{64}\alpha_p(R_{34} + R_{35}) - J_{74}R_{32}E_2,$
$J_{35} = R_{35} - J_{65}\alpha_p(R_{34} + R_{35}) - J_{75}R_{32}E_2,$
$J_{41} = R_{41} - J_{61}\alpha_p(R_{44} + R_{45}) - J_{71}R_{42}E_2,$
$J_{42} = R_{42} - J_{62}\alpha_p(R_{44} + R_{45}) - J_{72}R_{42}E_2,$
$J_{43} = R_{43} - J_{63}\alpha_p(R_{44} + R_{45}) - J_{73}R_{42}E_2,$
$J_{44} = R_{44} - J_{64}\alpha_p(R_{44} + R_{45}) - J_{74}R_{42}E_2,$
$J_{45} = R_{45} - J_{65}\alpha_p(R_{44} + R_{45}) - J_{75}R_{42}E_2,$
$J_{51} = R_{51} - J_{61}\alpha_p(R_{54} + R_{55}) - J_{71}R_{52}E_2,$
$J_{52} = R_{52} - J_{62}\alpha_p(R_{54} + R_{55}) - J_{72}R_{52}E_2,$
$J_{53} = R_{53} - J_{63}\alpha_p(R_{54} + R_{55}) - J_{73}R_{52}E_2,$
$J_{54} = R_{54} - J_{64}\alpha_p(R_{54} + R_{55}) - J_{74}R_{52}E_2,$
$J_{55} = R_{55} - J_{65}\alpha_p(R_{54} + R_{55}) - J_{75}R_{52}E_2,$
$J_{61} = -J_{66}E_3(R_{31} + (R_{41}S_1 + R_{51}(1 - S_1))\frac{\alpha_p}{\alpha_s}),$
$J_{62} = -J_{66}E_3(R_{32} + (R_{42}S_1 + R_{52}(1 - S_1))\frac{\alpha_p}{\alpha_s})),$
$J_{63} = -J_{66}E_3(R_{33} + (R_{43}S_1 + R_{53}(1 - S_1))\frac{\alpha_p}{\alpha_s})),$
$J_{64} = -J_{66}E_3(R_{34} + (R_{44}S_1 + R_{54}(1 - S_1))\frac{\alpha_p}{\alpha_s})),$
$J_{65} = -J_{66}E_3(R_{35} + (R_{45}S_1 + R_{55}(1 - S_1))\frac{\alpha_p}{\alpha_s})),$
$J_{71} = -J_{76}E_3(R_{31} + (R_{41}S_1 + R_{51}(1 - S_1))\frac{\alpha_p}{\alpha_s})),$
$J_{72} = -J_{76}E_3(R_{32} + (R_{42}S_1 + R_{52}(1 - S_1))\frac{\alpha_p}{\alpha_s})),$
$J_{73} = -J_{76}E_3(R_{33} + (R_{43}S_1 + R_{53}(1 - S_1))\frac{\alpha_p}{\alpha_s})),$
$J_{74} = -J_{76}E_3(R_{34} + (R_{44}S_1 + R_{54}(1 - S_1))\frac{\alpha_p}{\alpha_s})),$
$J_{75} = -J_{76}E_3(R_{35} + (R_{45}S_1 + R_{55}(1 - S_1))\frac{\alpha_p}{\alpha_s})),$
$J_{16} = -\frac{1}{\alpha_p}J_{66}(R_{14} + R_{15}) - J_{76}R_{12}E_2,$
$J_{17} = -\frac{1}{\alpha_p}J_{67}(R_{14} + R_{15}) - J_{77}R_{12}E_2,$
$J_{26} = -\frac{1}{\alpha_p}J_{66}(R_{24} + R_{25}) - J_{76}R_{22}E_2,$
$J_{27} = -\frac{1}{\alpha_p}J_{67}(R_{24} + R_{25}) - J_{77}R_{22}E_2,$
$J_{36} = -\frac{1}{\alpha_p}J_{66}(R_{34} + R_{35}) - J_{76}R_{32}E_2,$
$J_{37} = -\frac{1}{\alpha_p}J_{67}(R_{34} + R_{35}) - J_{77}R_{32}E_2,$
$J_{46} = -\frac{1}{\alpha_p}J_{66}(R_{44} + R_{45}) - J_{76}R_{42}E_2,$
$J_{47} = -\frac{1}{\alpha_p}J_{67}(R_{44} + R_{45}) - J_{77}R_{42}E_2,$
$J_{56} = -\frac{1}{\alpha_p}J_{66}(R_{54} + R_{55}) - J_{76}R_{52}E_2,$
$J_{57} = -\frac{1}{\alpha_p}J_{67}(R_{54} + R_{55}) - J_{77}R_{52}E_2,$
$n_{11} = -1 - \frac{E_3}{\alpha_p}(R_{34} + R_{35} + ((R_{44} + R_{45})S_1 + (R_{54} + R_{55})(1 - S1))\frac{\alpha_p}{\alpha_s}),$
$n_{12} = -(\frac{1-\alpha_f}{\alpha_s})E_3 - E_2E_3(R_{32} + (R_{42}S_1 + R_{52}(1 - S_1))\frac{\alpha_p}{\alpha_s}),$
$n_{21} = -\frac{1}{\alpha_f}, n_{22} = -\frac{1}{K_f}, J_{66} = \frac{n_{22}}{n_{11}n_{22}-n_{12}n_{21}}, J_{67} = -\frac{n_{12}}{n_{11}n_{22}-n_{12}n_{21}}, J_{76} = -\frac{n_{21}}{n_{11}n_{22}-n_{12}n_{21}},$
$J_{77} = \frac{n_{11}}{n_{11}n_{22}-n_{12}n_{21}},$

$$R_{44} = \frac{-K_1S_1(K_s^2\alpha_p(K_2+A_2/S_1)+A_1A_2(1-S_1)K_2/S_1)}{A_3}$$
$$R_{45} = \frac{K_1K_2(1-S_1)(-K_s^2\alpha_p+A_1A_2)}{A_3},$$
$$R_{54} = \frac{K_1K_2S_1(-K_s^2\alpha_p+A_1A_2)}{A_3},$$
$$R_{55} = \frac{-K_2(1-S_1)(K_s^2\alpha_p(K_1+\frac{A_2}{(1-S_1)})+\frac{A_1A_2S_1K_1}{(1-S_1)})}{A_3},$$
$$R_{41} = \frac{K_1(1-S_1)(K_s^2\alpha_p+A_1K_2)}{A_3},$$
$$R_{42} = \frac{K_{fr}(K_1K_s(A_2+K_2))}{A_3},$$
$$R_{43} = -\frac{\alpha_sK_1K_s^2(A_2+K_2)}{A_3},$$
$$R_{51} = -\frac{K_2S_1(K_1A_1+K_s^2\alpha_p)}{A_3},$$
$$R_{52} = \frac{K_{fr}(K_2K_s)(K_1+A_2)}{A_3},$$
$$R_{53} = \frac{\alpha_s(-K_2K_s^2(K_1+A_2))}{A_3},$$
$$R_{14} = \frac{A_1K_1S_1\alpha_p(A_2+K_2)}{A_3},$$
$$R_{15} = \frac{A_1K_2(1-S_1)\alpha_p(K_1+A_2)}{A_3},$$
$$R_{24} = \frac{-K_1S_1(1-S_1)(K_s^2\alpha_p+A_1K_2)}{A_3},$$
$$R_{25} = \frac{S_1(1-S_1)K_2(K_s^2\alpha_p+A_1K_1)}{A_3},$$
$$R_{34} = -\frac{K_1A_1K_s\alpha_pS_1(A_2+K_2)}{\alpha_sA_3},$$
$$R_{35} = \frac{-A_1K_2K_s^2\alpha_p(1-S_1)(K_1+A_2)}{\alpha_sK_sA_3},$$
$$R_{11} = \frac{A_1S_1(1-S_1)\alpha_p(K_2-K_1)}{A_3},$$
$$R_{12} = \frac{K_{fr}K_s\alpha_p(K_1(1-S_1)+A_2+K_2S_1)}{A_3},$$
$$R_{13} = \frac{-\alpha_sK_s^2\alpha_p(K_1(1-S_1)+A_2+K_2S_1)}{A_3},$$
$$R_{21} = \frac{\frac{-1}{P_{cap}}+(K_1K_s^2\alpha_p(1-S_1)+A_1K_1K_2+K_2S_1K_s^2\alpha_p)}{P_{cap}A_3},$$
$$R_{22} = \frac{S_1(1-S_1)K_sK_{fr}(K_1-K_2)}{A_3},$$
$$R_{23} = \frac{\alpha_sK_s^2S_1(1-S_1)(K_2-K_1)}{A_3},$$
$$R_{31} = \frac{A_1S_1(1-S_1)K_s^2\alpha_p(K_1-K_2)}{\alpha_sK_sA_3},$$
$$R_{32} = \frac{(\frac{-Kfr}{\alpha_p})+A_1K_{fr}(S_1K_1A_2+K_1K_2+K_2A_2(1-S_1))}{\alpha_sA_3},$$
$$R_{33} = \frac{A_1K_s(-(K_1A_2S_1+K_1K_2+A_2K_2(1-S_1)))}{A_3},$$
$$A_2 = S_1(1-S_1)\frac{dP_{cap}}{dS_1}$$
$$A_3 = A_1((1-S_1)A_2K_2+K_1K_2+K_1A_2S_1)+K_s^2\alpha_p(A_2+K_2S_1+K_1(1-S_1)),$$
$$E_2 = (1-\alpha_f)(\frac{1}{K_{fr}}-\frac{1}{K_{frm}}),$$
$$E_3 = F((\frac{\alpha_s}{K_s})-\frac{\alpha_s^2}{K_{fr}}),$$
$$A_1 = (\alpha_sK_s-K_{fr})-E_2K_{fr}K_s,$$
$$A_2 = S_1(1-S_1)\frac{dP_{cap}}{dS_1},$$
$$A_3 = A_1((1-S_1)A_2K_2+K_1K_2+K_1A_2S_1)+K_s^2\alpha_p(A_2+K_2S_1+K_1(1-S_1)),$$
$$E_1 = \frac{1}{K_s}-\frac{(1-\alpha_f)}{K_{frm}},$$
$$E_2 = (1-\alpha_f)(\frac{1}{K_{fr}}-\frac{1}{K_{frm}}),$$
$$E_3 = F((\frac{\alpha_s}{K_s})-\frac{\alpha_s^2}{K_{fr}}),$$
$$\alpha_p = \alpha_1+\alpha_2,$$
$$S_1 = \frac{\alpha_1}{\alpha_p}, S_2 = \frac{\alpha_2}{\alpha_p},\ F = 0.8.$$

Appendix B

$\Gamma_{11} = \frac{(a_{11}+2G_{fr})}{c^2} + G_{fr}q^2 - \langle\rho_s\rangle - e_1 - e_2 - e_3$, $\Gamma_{12} = (a_{11}+G_{fr})\frac{q}{c}$, $\Gamma_{13} = \left(e_1 + \frac{a_{12}}{c^2}\right)$, $\Gamma_{14} = a_{12}\frac{q}{c}$, $\Gamma_{15} = e_2 + \frac{a_{13}}{c^2}$, $\Gamma_{16} = a_{13}\frac{q}{c}$, $\Gamma_{17} = e_3 + \frac{a_{14}}{c^2}$, $\Gamma_{18} = a_{14}\frac{q}{c}$, $\Gamma_{21} = (a_{11}+G_{fr})\frac{q}{c}$, $\Gamma_{22} = \frac{G_{fr}}{c^2} + (2G_{fr} + a_{11})q^2 - \langle\rho_s\rangle - e_1 - e_2 - e_3$, $\Gamma_{23} = a_{12}\frac{q}{c}$, $\Gamma_{24} = e_1 + a_{12}q^2$, $\Gamma_{25} = a_{13}\frac{q}{c}$, $\Gamma_{26} = e_2 + a_{13}q^2$, $\Gamma_{27} = a_{14}\frac{q}{c}$, $\Gamma_{28} = e_3 + a_{14}q^2$, $\Gamma_{31} = e_1 + \frac{a_{21}}{c^2}$, $\Gamma_{32} = a_{21}\frac{q}{c}$, $\Gamma_{33} = \frac{a_{22}}{c^2} - e_1 - \langle\rho_1\rangle$, $\Gamma_{34} = a_{22}\frac{q}{c}$, $\Gamma_{35} = \frac{a_{23}}{c^2}$, $\Gamma_{36} = a_{23}\frac{q}{c}$, $\Gamma_{37} = \frac{a_{24}}{c^2}$, $\Gamma_{38} = a_{24}\frac{q}{c}$, $\Gamma_{41} = a_{21}\frac{q}{c}$, $\Gamma_{42} = e_1 + a_{21}q^2$, $\Gamma_{43} = a_{22}\frac{q}{c}$, $\Gamma_{44} = a_{22}q^2 - \langle\rho_1\rangle - e_1$, $\Gamma_{45} = a_{23}\frac{q}{c}$, $\Gamma_{46} = a_{23}q^2$, $\Gamma_{47} = a_{24}\frac{q}{c}$, $\Gamma_{48} = a_{24}q^2$,$\Gamma_{51} = e_2 + \frac{a_{31}}{c^2}$, $\Gamma_{52} = a_{31}\frac{q}{c}$, $\Gamma_{53} = \frac{a_{32}}{c^2}$, $\Gamma_{54} = a_{32}\frac{q}{c}$, $\Gamma_{55} = \frac{a_{33}}{c^2} - \langle\rho_2\rangle - e_2$, $\Gamma_{56} = a_{33}\frac{q}{c}$, $\Gamma_{57} = \frac{a_{34}}{c^2}$, $\Gamma_{58} = a_{34}\frac{q}{c}$, $\Gamma_{61} = a_{31}\frac{q}{c}$, $\Gamma_{62} = e_2 + a_{31}q^2$, $\Gamma_{63} = a_{32}\frac{q}{c}$, $\Gamma_{64} = a_{32}q^2$, $\Gamma_{65} = a_{33}\frac{q}{c}$, $\Gamma_{66} = a_{33}q^2 - \langle\rho_2\rangle - e_2$, $\Gamma_{67} = a_{34}\frac{q}{c}$, $\Gamma_{68} = a_{34}q^2$, $\Gamma_{71} = e_3 + \frac{a_{41}}{c^2}$, $\Gamma_{72} = a_{41}\frac{q}{c}$, $\Gamma_{73} = \frac{a_{42}}{c^2}$, $\Gamma_{74} = a_{42}\frac{q}{c}$, $\Gamma_{75} = \frac{a_{43}}{c^2}$, $\Gamma_{76} = a_{43}\frac{q}{c}$, $\Gamma_{77} = \frac{a_{44}}{c^2} - \langle\rho_f\rangle - e_3$, $\Gamma_{78} = a_{44}\frac{q}{c}$, $\Gamma_{81} = a_{41}\frac{q}{c}$, $\Gamma_{82} = e_3 + a_{41}q^2$, $\Gamma_{83} = a_{42}\frac{q}{c}$, $\Gamma_{84} = a_{42}q^2$, $\Gamma_{85} = a_{43}\frac{q}{c}$, $\Gamma_{86} = a_{43}q^2$, $\Gamma_{87} = a_{44}\frac{q}{c}$, $\Gamma_{88} = a_{44}q^2 - \langle\rho_f\rangle - e_3$.

Appendix C

$h_1 = l_{25}z_1$,
$h_2 = l_{25}z_2 + l_{26}z_1$,
$h_3 = l_{25}z_3 + z_2 l_{26}$,
$h_4 = l_{25}z_4 + l_{26}z_3$,
$h_5 = l_{25}z_5 + l_{26}z_4$,
$h_6 = l_{26}z_5$,

$l_{25} = G_{fr}$,
$l_{26} = e_1^2/s_2 + e_2^2/s_3 + e_3^2/s_4 - s_1$,

$z_1 = l_{17}y_1 - l_{22}y_5 + l_{23}y_9 - l_{24}y_{13}$,
$z_2 = l_{17}y_2 + l_{18}y_1 - l_{22}y_6 - l_{19}y_5 + l_{23}y_{10} + y_9 l_{20} - l_{24}y_{14} - l_{21}y_{13}$,
$z_3 = l_{17}y_3 + l_{18}y_2 - l_{22}y_7 - l_{19}y_6 + l_{23}y_{11} + l_{20}y_{10} - l_{24}y_{15} - l_{21}y_{14}$,
$z_4 = l_{17}y_4 + l_{18}y_3 - l_{22}y_8 - l_{19}y_7 + l_{23}y_{12} + l_{20}y_{11} - l_{24}y_{16} - l_{21}y_{15}$,
$z_5 = l_{18}y_4 - l_{19}y_8 + l_{20}y_{12} - l_{21}y_{16}$,

$s_1 = \langle\rho_s\rangle + e_1 + e_2 + e_3, s_2 = \langle\rho_1\rangle + e_1, s_3 = \langle\rho_2\rangle + e_2, s_4 = \langle\rho_f\rangle + e_3$,

$l_{17} = a_{11} + 2G_{fr}$,
$l_{18} = ((a_{11} + 2G_{fr})/c^2) - s_1$,
$l_{19} = a_{12} + c^2 e_1$,
$l_{20} = a_{13} + c^2 e_2$,
$l_{21} = a_{14} + c^2 e_3$,
$l_{22} = a_{12}c^2$,
$l_{23} = a_{13}c^2$,
$l_{24} = a_{14}c^2$,

$y_1 = l_1 c^6$,
$y_2 = (3l_1 + l_2)c^4$,
$y_3 = (3l_1 + 2l_2 + l_3)c^2$,
$y_4 = l_1 + l_2 + l_3 + l_4$,
$y_5 = l_5 c^6$,
$y_6 = c^4(3l_5 + l_6), y_7 = c^2(3l_5 + 2l_6 + l_7)$,

$y_8 = l_5 + l_6 + l_7 + l_8,$
$y_9 = l_9 c^6,$
$y_{10} = c^4(3l_9 + l_{10}),$
$y_{11} = c^2(3l_9 + 2l_{10} + l_{11}),$
$y_{12} = l_9 + l_{10} + l_{11} + l_{12},$
$y_{13} = l_{13} c^6,$
$y_{14} = c^4(3l_{13} + l_{14}),$
$y_{15} = c^2(3l_{13} + 2l_{14} + l_{15}),$
$y_{16} = l_{13} + l_{14} + l_{15} + l_{16},$

$l_1 = a_{23}(a_{42}a_{34} - a_{44}a_{32}) + a_{24}(a_{43}a_{32} - a_{42}a_{33}) + a_{22}(a_{44}a_{33} - a_{43}a_{34}),$
$l_2 = (s_4 a_{23} a_{32} + a_{24} a_{42} s_3 - a_{22}(s_4 a_{33} + s_3 a_{44}) - s_2(a_{33}a_{44} - a_{34}a_{43}))c^2,$
$l_3 = (s_3 s_4 a_{22} + s_2(s_4 a_{33} + s_3 a_{44}))c^4,$
$l_4 = -s_2 s_3 s_4 c^6,$
$l_5 = \frac{1}{c^2}\left(a_{24}(a_{43}a_{31} - a_{41}a_{33}) + a_{23}(a_{34}a_{41} - a_{44}a_{31}) + a_{21}(a_{44}a_{33} - a_{43}a_{34})\right),$
$l_6 = e_1(a_{33}a_{44} - a_{34}a_{43}) - a_{21}(s_4 a_{33} + s_3 a_{44}) + a_{23}(a_{33}s_4 + e_3 a_{34} - a_{44}e_2) + a_{24}(e_2 a_{43} - e_3 a_{33} + a_{41}s_3),$
$l_7 = c^2(s_3 s_4 a_{21} - e_1(s_4 a_{33} + s_3 a_{44}) + a_{23} e_2 s_4 + a_{24} s_3 e_3),$
$l_8 = e_1 s_3 s_4 c^4,$
$l_9 = \frac{1}{c^2}(a_{21}(a_{32}a_{44} - a_{34}a_{42}) + a_{22}(a_{41}a_{34} - a_{31}a_{44}) + a_{24}(a_{31}a_{42} - a_{32}a_{41})),$
$l_{10} = e_1(a_{32}a_{44} - a_{34}a_{42}) - a_{21}s_4 a_{32} + a_{22}(e_3 a_{34} + s_4 a_{31} - e_2 a_{44}) - s_2(a_{41}a_{34} - a_{31}a_{44}) + a_{24}(e_2 a_{42} - e_3 a_{32}),$
$l_{11} = c^2(-e_1 s_4 a_{32} + a_{22} e_2 s_4 - s_2(e_3 a_{34} + s_4 a_{31} - e_2 a_{44})),$
$l_{12} = -e_2 s_2 s_4 c^4,$
$l_{13} = \frac{1}{c^2}(a_{21}(a_{32}a_{43} - a_{33}a_{42}) + a_{22}(a_{41}a_{33} - a_{31}a_{43}) + a_{23}(a_{31}a_{42} - a_{32}a_{41})),$
$l_{14} = s_3 a_{21} a_{42} + e_1(a_{32}a_{43} - a_{33}a_{42}) + a_{22}(e_3 a_{33} - s_3 a_{41} - a_{43}e_2) - s_2(a_{41}a_{33} - a_{31}a_{43}) + a_{23}(e_2 a_{42} - e_3 a_{32}),$
$l_{15} = c^2(e_1 s_3 a_{42} - a_{22} e_3 s_3 - s_2(e_3 a_{33} - s_3 a_{41} - a_{31}e_2)),$
$l_{16} = e_3 s_2 s_3 c^4.$

References

1. Biot, M. A., Theory of propagation of elastic waves in a fluid-saturated porous solid. I. Low-frequency range. *The Journal of the Acoustical Society of America*, 28(2), 168–178, (1956a).
2. Biot, M. A., Theory of propagation of elastic waves in a fluid-saturated porous solid. II. Higher frequency range. *The Journal of the Acoustical Society of America*, 28(2), 179–191, (1956b).
3. Biot, M. A., Generalized theory of acoustic propagation in porous dissipative media. *The Journal of the Acoustical Society of America*, 34(9A), 1254–1264, (1962a).
4. Biot, M. A., Mechanics of deformation and acoustic propagation in porous media. *Journal of Applied Physics*, 33(4), 1482–1498, (1962b).
5. Plona, T. J., Observation of a second bulk compressional wave in a porous medium at ultrasonic frequencies. *Applied Physics Letters*, 36(4), 259–261, (1980).
6. Stoll, R. D., Kan, T.-K., Reflection of acoustic waves at a water–sediment interface. *The Journal of the Acoustical Society of America*, 70(1), 149–156, (1981).
7. Dutta, N. C., Ode, H., Seismic reflections from a gas-water contact. *Geophysics*, 48(2), 148–162, (1983).
8. Garg, S. K., Nayfeh, A. H., Compressional wave propagation in liquid and/or gas saturated elastic porous media. *Journal of Applied Physics*, 60(9), 3045–3055, (1986).
9. Wu, K., Xue, Q., Adler, L., Reflection and transmission of elastic waves from a fluid-saturated porous solid boundary. *The Journal of the Acoustical Society of America*, 87(6), 2349–2358, (1990).
10. Denneman, A. I., Drijkoningen, G. G., Smeulders, D. M., Wapenaar, K., Reflection and transmission of waves at a fluid/porous-medium interface. *Geophysics*, 67(1), 282–291, (2002).
11. Dai, Z.-J., Kuang, Z.-B., Reflection and transmission of elastic waves at the interface between water and a double porosity solid. *Transport in Porous Media*, 72, 369–392, (2008).
12. Vashishth, A. K., Sharma, M. D., Reflection and refraction of acoustic waves at poroelastic ocean bed. *Earth, Planets and Space*, 61, 675–687, (2009).
13. Sharma, M. D., Wave-induced flow of pore fluid in a double-porosity solid under liquid layer. *Transport in Porous Media*, 113, 531–547, (2016).

14. Geng, H., Ding, H., Liu, J., Cui, Z., Kundu, T., Reflection and refraction of plane waves at an interface of water and porous media with slip boundary effect. *Transport in Porous Media*, 148(1), 173–190, (2023).

15. Tuncay, K., Corapcioglu, M. Y., Body waves in poroelastic media saturated by two immiscible fluids. *Journal of Geophysical Research: Solid Earth*, 101(B11), 25149–25159, (1996).

16. Tuncay, K., Corapcioglu, M. Y., Wave propagation in poroelastic media saturated by two fluids. *Journal of Applied Mechanics*, 64, 313–320, (1997).

17. Tuncay, K., Corapcioglu, M. Y., Wave propagation in fractured porous media. *Transport in Porous Media*, 23, 237–258, (1996a).

18. Tuncay, K., Corapcioglu, M. Y., Body waves in fractured porous media saturated by two immiscible newtonian fluids. *Transport in Porous Media*, 23, 259–273, (1996b).

19. Tomar, S., Arora, A., Reflection and transmission of elastic waves at an elastic/porous solid saturated by two immiscible fluids. *International Journal of Solids and Structures*, 43(7-8), 1991–2013, (2006).

20. Arora, A., Tomar, S., Seismic reflection from an interface between an elastic solid and a fractured porous medium with partial saturation. *Transport in Porous Media*, 85, 375–396, (2010).

21. Sharma, M. D., Kumar, M., Reflection of attenuated waves at the surface of a porous solid saturated with two immiscible viscous fluids. *Geophysical Journal International*, 184(1), 371–384, (2011).

22. Achenbach, J., *Wave propagation in elastic solids*. Elsevier, (2012).

Anil K. Vashishth
Department of Mathematics,
Kurukshetra University, Kurukshetra - 136119, Haryana
India.
Orcid Id: https://orcid.org/0000-0001-5511-9306

and

Sourab Kamboj
Corresponding Author
Department of Mathematics,
Kurukshetra University, Kurukshetra - 136119, Haryana
India.
E-mail address: mathsourab11020@kuk.ac.in
Orcid Id: https://orcid.org/0009-0009-6876-1125